Science of the Total Environment 822 (2022) 153343

Contents lists available at ScienceDirect

Science of the Total Environment

journal homepage: www.elsevier.com/locate/scitotenv

Inter-comparisons of mean, trend and interannual variability of global terrestrial gross primary production retrieved from remote sensing approach

Jiaqi Dong [a], Longhui Li [b,c,d,*], Yuzhen Li [e], Qiang Yu [a,**]

[a] State Key Laboratory of Soil Erosion and Dryland Farming on the Loess Plateau, Northwest A & F University, Yangling 712100, China
[b] Key Laboratory of Virtual Geographical Environment of Ministry of Education, Nanjing Normal University, Nanjing 210023, China
[c] Jiangsu Centre for Collaborative Innovation in Geographical Information Resource Development and Application, Nanjing 210023, China
[d] School of Geographical Sciences, Nanjing Normal University, Nanjing 210023, China
[e] School of Emergency Management, Xihua University, Chengdu 610039, China

HIGHLIGHTS

- Eight GPP products generated by remote sensing approach were inter-compared
- Long-term global multiple-year mean GPP varied from 128.5 to 158.3 Pg C $year^{-1}$ for eight models
- Trends in global total annual GPP from eight products varied from −0.22 to 0.51 Pg C $year^{-1}$
- Global mean interannual variability ranged from 0.10 to 0.35 for eight products

GRAPHICAL ABSTRACT

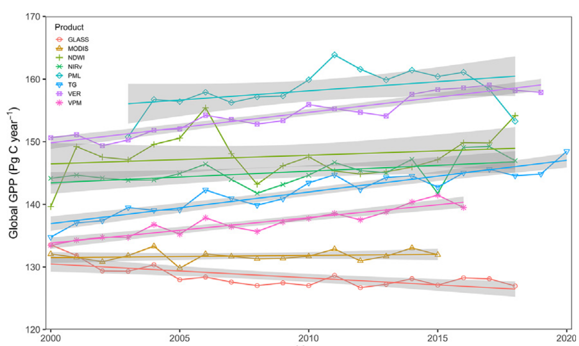

ARTICLE INFO

Article history:
Received 14 October 2021
Received in revised form 18 January 2022
Accepted 19 January 2022
Available online 29 January 2022

Editor: Elena Paoletti

Keywords:
Gross primary production
Inter-model comparisons
Light use efficiency

ABSTRACT

Many models were established to estimate gross primary production (GPP) of terrestrial ecosystems based on vegetation light use efficiency (LUE). Analysing the spatial-temporal variations of global terrestrial GPP became capable with the increasing length of satellite data. Previous studies mainly focused on evaluating the model performance or investigating the mean, the temporal trend or the interannual variability (IAV) of global terrestrial GPP based on one single or multiple models, which is difficult to identify common merits of a same cluster of GPP models. This study compared eight satellite-based LEU-type GPP models in capturing the mean, temporal trend and IAV of global GPP concurrently. Our results showed that current common-used models based on LUE methodology estimated global mean GPP ranging from 128.5 to 158.3 Pg C $year^{-1}$, and global mean IAV ranging from 0.1 to 0.35, but the trends ranging from −0.22 to 0.51 Pg C $year^{-1}$. In the context of plant functional types (PFTs) and climate classifications, no consistent feature for either of the mean, trend or IAV of GPP are identified among eight models. Future studies should integrate the latest advances on the mechanisms and associated environmental factors into models and consolidate performance of models to better understand the evolutions of terrestrial ecosystem functioning.

1. Introduction

Terrestrial gross primary production (GPP) is the major driver of global carbon cycle and it plays a vital role in regulating the atmospheric CO_2 concentration by partly offsetting anthropogenic CO_2 emissions (Canadell et al., 2007; Cox and Jones, 2008). Ecosystem GPP cannot be measured directly, and is commonly estimated using models,

* Correspondence to: L. Li, Key Laboratory of Virtual Geographical Environment of Ministry of Education, Nanjing Normal University, Nanjing 210023, China.
** Corresponding author.
E-mail addresses: 09410@njnu.edu.cn (L. Li), yuq@nwafu.edu.cn (Q. Yu).

http://dx.doi.org/10.1016/j.scitotenv.2022.153343

including physically process-based and semi-empirically satellite-based approaches (Krinner et al., 2005; Sims et al., 2008; Wang et al., 2010; Yuan et al., 2007).

Physically process-based models, commonly termed as land surface models (LSMs), are generally designed to describe the vegetation photosynthesis indicated by soil and atmospheric variables (Bonan et al., 2011). The most significant advantage of using LSMs lies in the continuousness of modeled GPP in both space and times, as the input data of LSMs can be generated at various spatiotemporal resolutions. LSMs also have advantages in implementing independently (offline) (Bonan et al., 2011; Dai et al., 2003; Krinner et al., 2005) or coupling with climate model (online, also termed Earth System Model) (Law et al., 2015; Zeng et al., 2002). Therefore, LSMs have been intensively used to investigate the trend of GPP in long term period and at larger scales (Anav et al., 2015; Sitch et al., 2015). The disadvantage of LSMs is that a model has many parameters and most of them are difficult to determine from observations (Williams et al., 2009). LSMs also require multiple inputs including meteorological variables, vegetation, and soil maps, often with high spatial heterogeneities and large uncertainties.

The ecophysiological process of vegetation photosynthesis, i.e. GPP, is the conversion of solar energy absorbed by leaves into chemical energy in the presence of water and nutrition. At ecosystem scales, vegetation GPP is found to be directly or indirectly related to lots of parameters, including fluorescence (Rascher et al., 2015), Near Infrared Reflectance (NIRv) (Badgley et al., 2019; Badgley et al., 2017), Photosynthetically Active Radiation (PAR) (Xiao et al., 2004), Normalized Difference Vegetation Index (NDVI) (Yuan et al., 2007) or Enhanced Vegetation Index (EVI) (Sims et al., 2008; Sims et al., 2006), and Leaf Area Index (LAI) (Schaefer et al., 2008). All these parameters can be retrieved from satellite imagery, which provides basis and potential for estimating terrestrial GPP at global scale. As vegetation GPP is primarily limited by one or multiple factors, such as light, water, and nutrition, various GPP models are developed by integrating one or more of above-mentioned parameters. Among existing models, a cluster of light use efficiency (LUE) models has received many attentions. These LUE-type models described GPP as a product of multiple variables including PAR, fraction of PAR absorbed by the vegetation (*f*PAR), maximum LUE (LUE_{max}) and environmental constraints on LUE_{max}, such as water and nutrition (Landsberg and Waring, 1997; Potter et al., 1993; Yuan et al., 2014; Yuan et al., 2007). Some LUE GPP models also require ancillary environmental variables, such as air temperature, vapor pressure deficit, soil moisture, canopy water content, or canopy chlorophyll content, to constrain LUE_{max} (Yuan et al., 2014; Yuan et al., 2007). In LUE models, *f*PAR is generally formulated as a function of NDVI or EVI (Myneni and Williams, 1994; Zhang et al., 2017). Due to their simple framework and relatively fewer driving variables, LUE-type GPP models are frequently used to estimate terrestrial GPP, particularly at global scale and over long term periods.

Using LSMs or LUE models, current estimates of mean annual GPP of the global terrestrial ecosystems has a wide range from 90 to 175 Pg C $year^{-1}$ (Wang et al., 2012; Wang et al., 2021b; Zheng et al., 2020). The wide range of estimates are mainly resulted from model structure or process, i.e., which variables are considered to impact GPP and how their relationships are formulated in responding to a specific variable, and the variations in model parameters and input data (Li et al., 2020; Williams et al., 2009; Zhao et al., 2012). For a long term period, the trend in terrestrial GPP and its drivers are particularly important (Sitch et al., 2013), as this reflects the ability of terrestrial ecosystem in sequestrating CO_2 from the atmosphere. Recent studies suggested that atmospheric CO_2 concentration, nitrogen deposition, and related human land-use management have caused the increase in global LAI (Chen et al., 2019a; Zhu et al., 2016) and thus the global GPP (Chen et al., 2019b). However, it is also reported that global terrestrial GPP tends to decline due to the negative effect of atmospheric vapor pressure deficit (Yuan et al., 2019) or increase with a slower rate due to the weakening of CO_2 fertilization effect (Wang et al., 2020). Such wide range of estimates and inconsistent trends in global GPP requires us to further investigate how global GPP changed during the past few decades. Lots of studies have compared the global terrestrial GPP based on estimates from LSMs and LUE-type models, but mainly focused on the trends or the means of GPP (Zhang et al., 2019b; Zhang et al., 2017; Zheng et al., 2020). Except for the trend and mean, the IAV of global GPP is also important for us to understand the dynamics and evolutions of terrestrial ecosystems (Ahlström et al., 2015; Poulter et al., 2014). Therefore, investigating the mean, trend and IAV of global terrestrial GPP concurrently is urgently required.

The main objective of this research is to conduct a comprehensive intercomparison of mean, trend and IAV of global GPP estimated from several LUE-type models which are mainly driven by satellite data. The analysis is further categorized into different plant functional types (PFTs) and climate zones, the ultimate purpose is to provide an advanced understanding on how global terrestrial GPP evolved during the past 20 years and to guide the improvement of LUE-type models for estimating GPP. We hypothesize that currently satellite-based GPP models can consistently reproduce the mean and IAV of global GPP, but may show large discrepancy in the estimated trends. In addition, we also hypothesize that inter-model differences in the mean, IAV or trend are significant for a same PFT or climate zone but differences among PFTs or climate zones can be well captured by models.

2. Materials and methods

2.1. Global GPP products

Eight LUE-type GPP products (GLASS, MODIS, NDWI, NIRv, PML, TG, VER and VPM) are adopted for analysis in this research. The lengths of these GPP products ranged from 16 to 21 years. Descriptions on the product algorithm listed in Table 1 indicated that the GLASS GPP is constructed based on a "two-leaf" concept and other GPP products are established based on a "big-leaf" concept.

The GLASS GPP is developed by Zheng et al. (2020), in which a two-leaf (sunlit leaves and shaded leaves) LUE model is driven by absorbed PAR (APAR), atmospheric CO_2 concentration (C_s), air temperature (T_a) and vapor pressure deficit (VPD). The joint effects of C_s, T_a and VPD are used

Table 1
Temporal coverage, tempo-spatial resolutions and key algorithms of eight GPP products.

GPP product	Start year	End year	Total years	Spatial resolution	Temporal resolution	Product algorithm	References
GLASS	2000	2018	19	0.05°×0.05°	8 days	$(\varepsilon_{su} \times APAR_{su} + \varepsilon_{sh} \times APAR_{sh}) \times C_s \times \min(T_s, W_s)$	Zheng et al. (2020)
MODIS	2000	2015	16	0.05°×0.05°	Monthly	$\varepsilon \times PAR \times fPAR \times f(T_{min}, VPD)$	Running et al. (2004)
NDWI	2000	2018	19	0.08°×0.08°	Monthly	$\varepsilon_{max} \times PAR \times fPAR \times fCI \times fCO_2 \times \min(T_s, W_{s\_NDWI})$	Wang et al. (2021)
NIRv	2000	2018	19	0.05°×0.05°	Monthly	$f(NIR_v)$[a]	Wang et al. (2021)
PML	2003	2018	16	500 m×500 m	8 days	$f(VPD)A_{c,g}$[b]	Zhang et al. (2019a, 2019b)
TG	2000	2020	21	0.05°×0.05°	Monthly	$m \times EVI_{scaled} \times LST_{scaled}$	Sims et al. (2008)and Dong et al. (2017)
VER	2000	2019	20	0.10°×0.10°	10 days	$f(LAI, fPAR, R_s, T_a, RH, PFT, LAI_{min}, LAI_{max})$[c]	Zeng et al. (2020)
VPM	2000	2016	17	500 m×500 m	8 days	$\varepsilon_{max} \times FPAR \times PAR \times W_S \times T_S$	Zhang et al. (2017)

[a] Vegetation-specific linear regressions with NIR_v was used to estimate GPP.
[b] GPP was estimated from a coupled photosynthesis and transpiration model based on the Penman-Monteith equation.
[c] A random forest algorithm was used to estimate GPP.

to constrain the maximum LUE for both sunlit and shaded leaves, and APAR for sunlit and shaded leaves are scaled by LAI. T_a, VPD, PAR data are from MERRA-2 datasets (https://gmao.gsfc.nasa.gov/reanalysis/MERRA-2), and the LAI is obtained from the GLASS datasets (http://www.glass.umd.edu/Download.html). The GLASS GPP has a spatial resolution of 0.05° × 0.05° and temporal resolution of 8 days.

The MODIS GPP with an early version (MOD17A2) is derived from NASA MODIS website. In the MODIS GPP, LUE is calculated as the product of the maximum LUE with the scalars of air temperature and VPD. And APAR is calculated as a function of MODIS NDVI. The detailed procedures of estimating GPP is referred to Running et al. (2004). The MODIS GPP has a spatial resolution of 0.05° × 0.05° and a temporal resolution of a month.

The NDWI GPP is derived from Wang et al. (2021b). NDWI GPP considered multiple variables including water, temperature, cloudiness, and atmospheric CO_2 centration as constraints on GPP. A unique feature of the NDWI model is that the normalized difference water index (NDWI) is introduced as a water stress factor for GPP and NDWI can be directly retrieved from satellite observations. The NDWI GPP product has a spatial resolution of 0.08° × 0.08° and a temporal resolution of a month.

The NIRv GPP used the satellite-based near infrared reflectance (NIRv) to estimate GPP (Wang et al., 2021a). The NIRv GPP is mainly driven by the long-term observations of AVHRR reflectance data and calibrated with 104 eddy covariance (EC) sites from the global FLUXNET. The NIRv GPP was proven to have better abilities to capture the seasonal and inter-annual variations of terrestrial GPP at the global scale. The NIRv GPP has a spatial resolution of 0.05° × 0.05° and a temporal resolution of a month.

The PML GPP is generated by integrating a surface conductance model to the Penman-Monteith equation, and its original objective is to estimate ecosystem evapotranspiration (ET) using MODIS datasets (Zhang et al.,

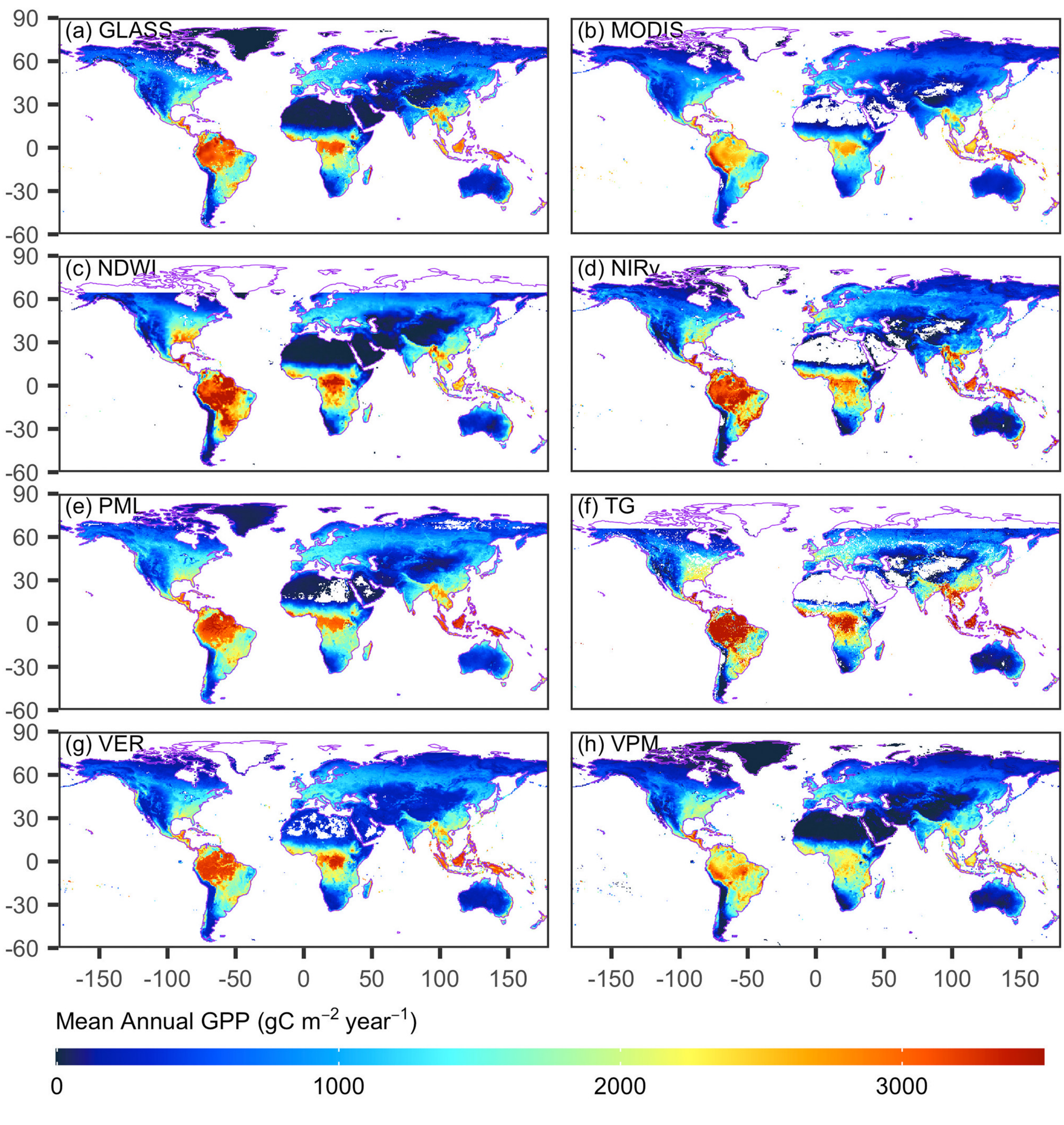

Fig. 1. Spatial distributions of mean annual GPP of eight global GPP products. For better visualization, values larger than 99% (smaller than 1%) quantile of mean annual GPP are set as the 99% quantile (1% quantile).

2016). Later, the model used a water-carbon coupled canopy conductance model to estimate ET and GPP simultaneously (Zhang et al., 2019b). VPD is also included to constrain GPP in the PML dataset. Multiple MODIS datasets including LAI, albedo and emissivity are used to drive the PML model. The PML GPP has a spatial resolution of $0.05^\circ \times 0.05^\circ$ and a temporal resolution of 8 days.

The TG GPP is generated in this research. Its algorithm is based on the "Temperature-Greenness" (TG) model original developed by Sims et al. (2008), but model's parameters were optimized by a Bayesian technique using 624 site-years of EC data from the global FLUXNET (Dong et al., 2017). Spatial parameters of the TG model are up-scaled based on MODIS land cover map (MCD12C1) in 2010. Required input data for the TG model consists of land surface temperature (LST) and EVI, which are from MOD11C3 and MOD13C2, respectively. The global TG model is run for each of the $0.05^\circ \times 0.05^\circ$ grid for each month. A unique feature of the TG model is that it is a purely remote sensing driving model and does not require any ancillary climatic, soil or vegetation data.

The VER GPP is a product generated by upscaling global FLUXNET data based on a random forest approach (Zeng et al., 2020). Satellite images including LAI and *f*APAR, and ancillary climate data including T_a, relative humidity, and downward shortwave solar radiation from ERA5 were jointly used to train the random forest to upscale GPP from FLUXNET site to the globe and make long-term predictions. A unique feature of the VER GPP is that three variants of LAI were used to represent PFTs so that measurements from different PFTs can be mixed better by the model and the GPP estimates are expected to have higher accuracy. The spatial and temporal resolutions are $0.1^\circ \times 0.1^\circ$ and 10 days, respectively.

The VPM model calculates GPP as the product of light absorption by chlorophyll of the vegetation ($APAR_{chl}$) and the efficiency (LUE) that converts the absorbed energy to carbon fixed by plants, in which $APAR_{chl}$ is further calculated as a product of PAR and the fraction of PAR absorbed by chlorophyll ($fPAR_{chl}$) and $fPAR_{chl}$ is calculated as a linear function of EVI. Actual LUE is down-regulated by temperature and water stress from its maximum value (LUE_{max}) (Zhang et al., 2017). LUE_{max} is defined from a biome specific lookup table. The VPM GPP dataset is available at $0.05^\circ \times 0.05^\circ$ spatial resolution and 8-day temporal resolution.

Meteorological variables are required to drive the GPP models for six out of eight products (except NIR_v and TG) according to literature listed in Table 1. The default temporal and spatial resolutions of each GPP product is resampled at $0.5^\circ \times 0.5^\circ$ grid pixel for each monthly for fair comparison based on the bilinear approach.

2.2. PFTs and Köppen-Geiger climate classifications

The MODIS land cover map (MCD12C1) in 2010 is used to drive the TG model, and to compare the mean, trend and IAV of GPP for different land cover classifications. The IGBP land cover scheme of MCD12C1 includes 17 land cover classes and 12 vegetation-related classes are used in this study. The 12 land cover maps consist of evergreen needle-leaf forest (ENF), evergreen broadleaf forest (EBF), deciduous needle-leaf forest (DNF), deciduous broadleaf forest (DBF), mixed forest (MF), closed shrublands (CSH), open shrublands (OSH), woody savannas (WSA), savannas (SAV), grasslands (GRA), permanent wetlands (WET) and croplands (CRO). The remaining 5 classes are considered as very low GPP and ignored. The original product of MCD12C1 has a spatial resolution of 500 m and this original spatial resolution of data is used to drive the TG model but is resampled into $0.5^\circ \times 0.05^\circ$ resolution to compare with other GPP products.

The Köppen-Geiger climate classification (Peel et al., 2007) was used to compare GPP in different climate zones. In the Köppen-Geiger climate classification, there are five major climate zones, named Tropical (A), Arid (B), Temperate (C), boreal (D), and Polar (E). Each major climate zone is divided into 2 to 12 sub-zones with different humidity conditions.

2.3. Calculation of mean, trend and interannual variability

Mean annual GPP was computed as the averaged value of annual GPP for each pixel during each estimation periods (16–21 years). Linear trend of mean annual GPP over quasi-two decades are computed for each grid using linear regression analysis, and the slope of the linear regression is defined as the trend of GPP. The interannual variability (IAV) was identified by the coefficient of variation (CV). As temporal coverages for different GPP products varied from each other, the mean, trend and IAV were calculated for each product over their own temporal coverage (see Table 1).

3. Results

3.1. Mean annual GPP

Fig. 1 shows the spatial distributions of mean annual GPP from eight GPP products (GLASS, MODIS, NDWI, NIRv, PML, TG, VER and VPM). It is clear that all eight products show quite similar spatial patterns of GPP at the global. High values of GPP are distributed at tropical rainforests (Amazon, Central Africa and South Asia) with annual GPP larger than 2000 gC m^{-2} $year^{-1}$. Low GPP values are distributed at arid or semiarid regions (North Africa, Central Asia and Central Australia) and high latitudes with annual GPP smaller

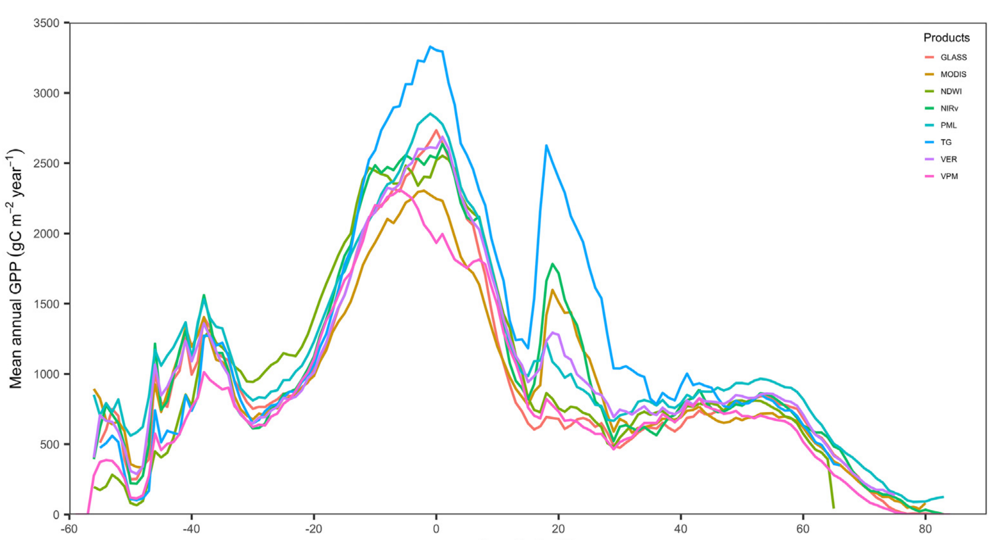

Fig. 2. Zonal profiles of mean annual GPP from eight GPP products.

than 200 gC m^{-2} year^{-1}. However, markable differences exist among eight products. For example, TG shows significant higher GPP than other seven products in Amazon regions and part of Central Africa. In contrast, VPM shows relatively low GPP in tropical rainforest regions.

Per-pixel comparisons among eight GPP products demonstrate high consistency of simulated mean annual GPP (R varying from 0.9 to 0.96, all significant at 0.001 level), though inconsistency can be seen from some pair of products. For example, pixel-by-pixel comparisons between TG and VPM show relatively large differences when mean annual GPP exceed 2500 gC m^{-2} year^{-1}. This inconsistency mainly occurs at tropical rainforest as showed in Fig. 1. majority inconsistencies among eight GPP products are sourced from either low (<200 gC m^{-2} year^{-1}) or high (2500 gC m^{-2} year^{-1}) GPP according to the histogram of mean annual GPP for each product (shown in diagonal panels in Fig. S1).

In order to perceive the main discrepancy among eight GPP products, we compared the zonal means annual GPP in Fig. 2. The latitudinal values of mean annual GPP are all peaked around the equator (10°S–10°N) and a second peak at 20°N expect GLASS and VPM. of the disappearance of second peak in zonal GPP of GLASS and VPM are largely caused by the fact that both GLASS and VPM estimated valid GPP although very small or zero in Sahara desert (Fig. 1), which causes low zonal mean GPP for these two products. Particularly, TG product shows a considerably higher double-peaks in GPP, comparing to other seven products. The large peak in GPP for all products reflects the wealth of climatic and nutrition resources in the equatorial regions, while the secondary peak in GPP for five out of eight products reflects high terrestrial ecosystem production in Mexico, India and south Asia. In contrast, all eight products show relatively low zonal mean GPP in the temperate regions of the two hemispheres and lowest in dry tropics (10°S–25°S and 10°N–25°N), due to the stress from water deficit. The GPP peak of TG is 1.5 times larger than that of MODIS. This large discrepancy of GPP among eight products is also found in the secondary peak intervals. However, GPP differences among the eight products in the temperate and dry regions are much smaller.

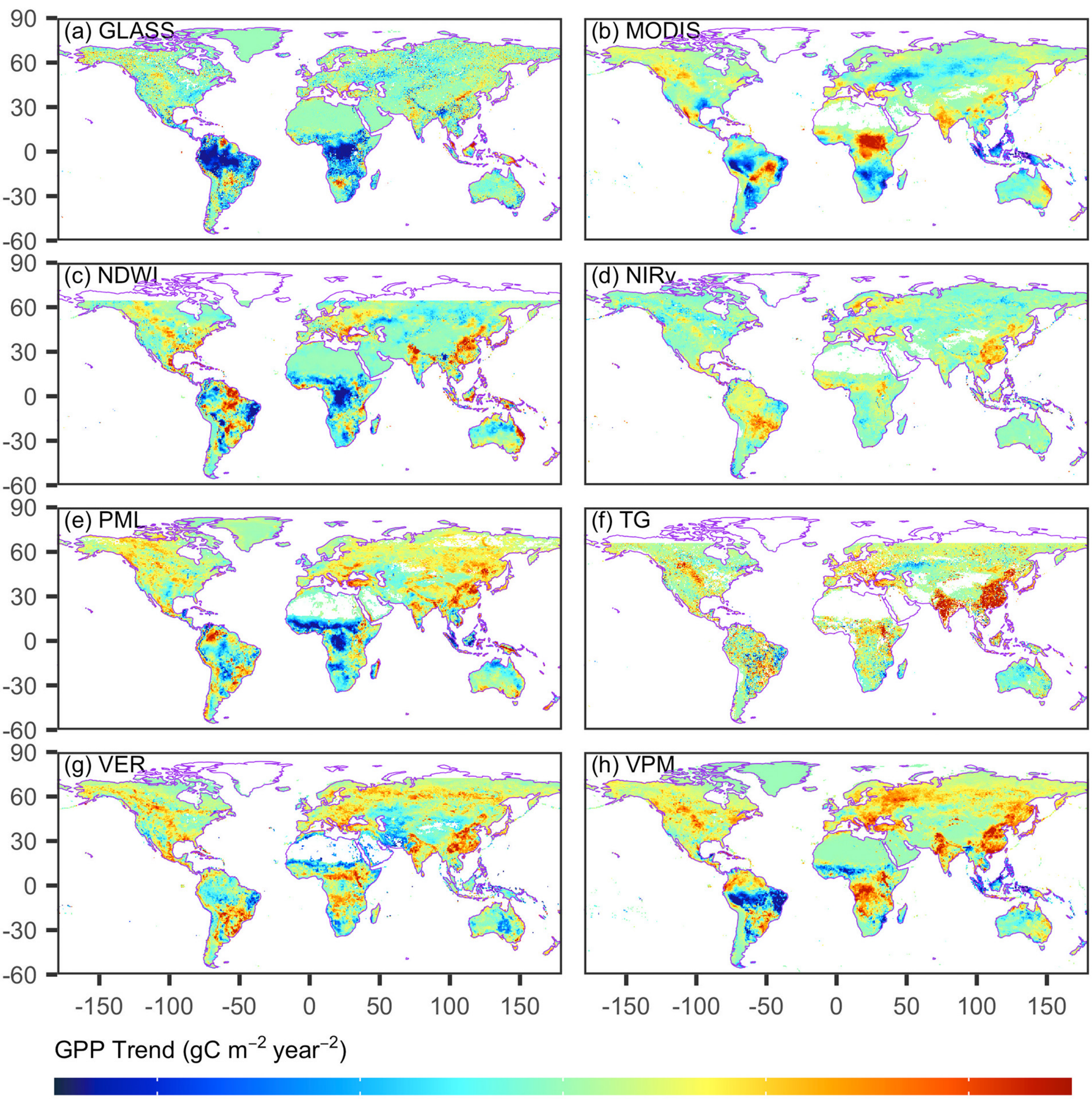

Fig. 3. Spatial distributions of GPP trends of eight products. For better visualization, values larger than 99% (smaller than 1%) quantile of mean annual GPP are set as the 99% quantile (1% quantile).

3.2. Trend of GPP

The trend of GPP for eight products is shown in Figure 3. Generally, all products predict an increased trend of GPP at most global terrestrial ecosystems, particularly in the northern hemisphere. However, few products show decreased trend of GPP in some regions. In detail, GLASS, MODIS, NDWI and VPM predict decreased GPP in part of Amazon rainforest, while GLASS, NDWI and PML estimate decreased GPP in central Africa, but MODIS gives increased trend. Deforestations and stress from atmospheric vapor pressure deficit (Yuan et al., 2019) may be the main reasons caused the GPP decreases during the past two decades. All GPP products show significant increased GPP in India and southeast China where vegetation greening is recently reported (Chen et al., 2019a; Zhu et al., 2016), although the magnitude of increasing trend varies among eight products.

At the global scale, per-pixel comparisons of the GPP trend are shown in Fig. S2. There are large discrepancy among eight GPP products. The correlation coefficient (R) among eight products ranges from 0.12 (GLASS vs MODIS) to 0.52 (VER vs VPM). The difference are also obvious from the shapes of histograms of GPP trend for each product. Particularly, GLASS product estimates large regions with decreased GPP in Amazon and central Africa during the past two decades, which makes the predicted GPP trend in GLASS largely differ from any other ones ($R < 0.26$). Similarly, PML also predicts decreased GPP in part of the equatorial zones, and the correlation coefficient (R) between the PML and other products is also lower than 0.36. Predicted trends of GPP from TG agree relatively well with those from NIRv, VER and VPM, with R values of 0.43, 0.48 and 0.46, respectively. All these facts indicate that representation of the trends of GPP is full of large challenge based on remote sensing approaches, although it is appreciated that same remote sensing variable is used or similar model construction strategy for GPP is adopt.

When summing up all grids GPP to calculate global annual GPP, all products except GLASS show decreased trend of annual global GPP (Figure 4). Three products, TG, VER and VPM, exhibit significant increasing trends of GPP with 0.49, 0.49, 0.41 Pg C year^{-1} ($p < 0.001$), respectively. NIRv also predicts significant increasing GPP trend with 0.19 Pg C year^{-1} ($p < 0.05$), but the other three GPP products, MODIS, NDWI and PML reproduce slightly positive but insignificant trends with 0.03, 0.14 and 0.29 Pg C year^{-1} ($p > 0.1$). The GLASS product generated a significant negative trend of GPP (-0.22 Pg C year^{-1}, $p < 0.001$).

3.3. IAV of GPP

IAV is another important indicator to describe the feature of the long-term variations in terrestrial GPP in addition to the mean and trend of GPP. Generally, larger IAV of GPP are mainly located in arid and semiarid regions, such as in Australia, central Asia, western of US and south of Africa, which agreed well with previous report (Poulter et al., 2014). However, significant discrepancy of GPP IAV existed among eight GPP products. For example, GLASS and NDWI products showed more areas of high GPP IAV (Fig. 5a,c), compared to other products. In contrast, MODIS showed much lower GPP IAV (Fig. 5b).

Inter-comparisons of GPP IAV between eight products showed quite large differences. The correlation coefficient (upright of Fig. S3) ranges from 0.26 between VER and GLASS to 0.7 between VPM and TG (Fig. S3). Relatively high correlation coefficient values (>0.6) are found between TG and VPM (0.66), MODIS and VER (0.62), MODIS and PML (0.6). Relatively low correlation coefficient values (<0.3) are found between VER and GLASS (0.18), VPM and GLASS (0.22), NDWI and MODIS (0.24), NIRv and MODIS (0.27), VER and NDWI (0.25) and VER and NIRv (0.24) (Fig. S3).

3.4. GPP variations in different biome types and climate zones

Although the trend and IAV of GPP show similar spatial patterns at the global scale, substantial differences in GPP exist among models at 0.5×0.5 degree pixel level. To testify if there are significant GPP discrepancies among PFT and oror climatic zones, we calculated the mean, trend and IAV of GPP from all products for each IGBP PFT and Köppen-Geiger climate zones.

For 12 PFTs, EBF has the largest gross primary production with a mean annual GPP of multiple products with 2860 ± 346 gC m^{-2} year^{-1} and OSH has the smallest GPP with 327 ± 75 gC m^{-2} year^{-1} (Fig. 6a). The other five PFTs, i.e. DBF, SAV, WSA, MF and CRO have mean annual GPP larger than 1000 gC m^{-2} year^{-1}, and GRA and OSH showed mean annual GPP smaller than 500 gC m^{-2} year^{-1}. Overall, all GPP products well captured such

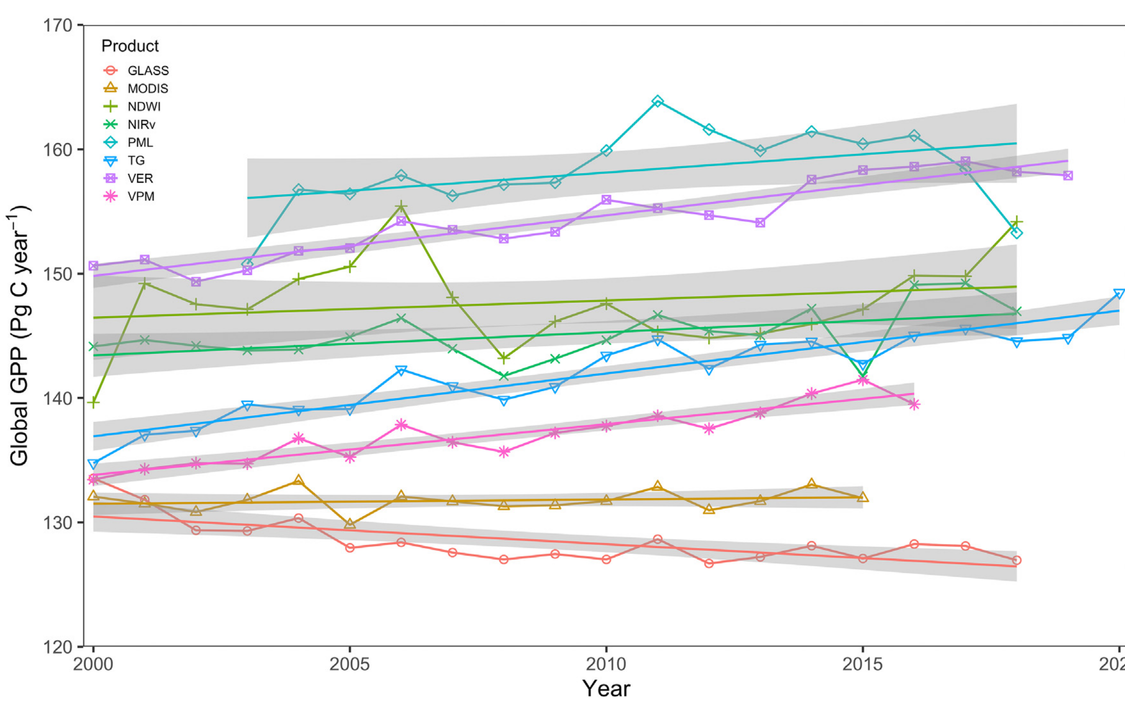

Fig. 4. The global average annual total GPP (Pg C year^{-1}) trends of the eight products calculated by linear regression analysis.

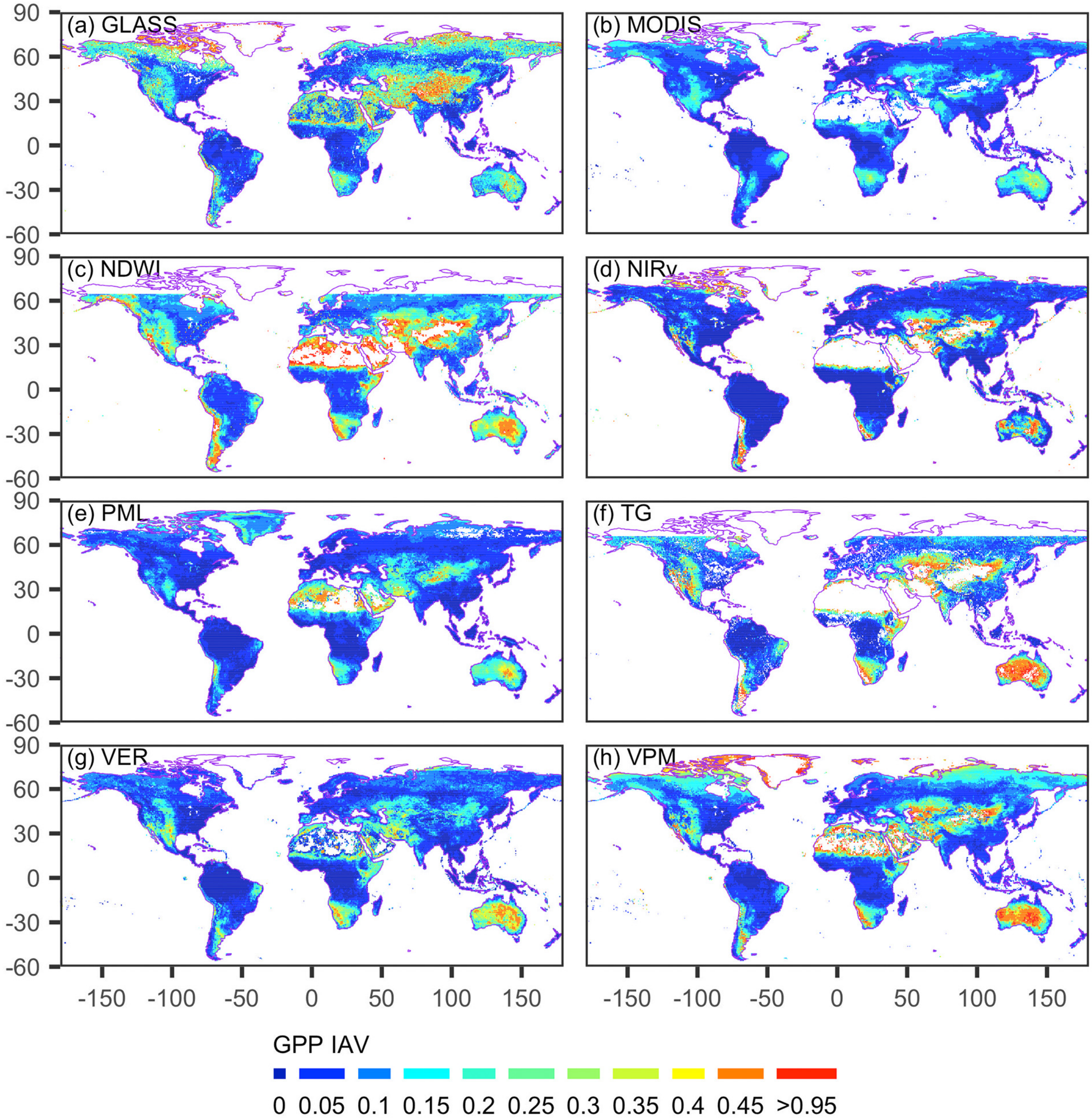

Fig. 5. Spatial distributions of GPP interannual variability (IAV) of eight products. For better visualization, values larger than 99% (smaller than 1%) quantile of GPP interannual variability are set as the 99% quantile (1% quantile).

differences among PFTs and the difference among products is moderate (Fig. 6a).

Simulated GPP trends for 12 PFTs from eight products ranged from -10 gC m^{-2} year^{-1} to 9.33 gC m^{-2} year^{-1} (Fig. 6b). For CRO, ENF and MF, all eight products predicted increased trends in GPP. For the remaining PFTs, some products predicted increased GPP trends, but others predicted decreased trends (Fig. 6b). Among the 12 PFTs, the differences in simulated GPP trends are quite large, particularly for EBF and SAV. Such differences in GPP trends among products for different PFT further confirms the high uncertainties of predicted trends of GPP from different products as shown in Figs. 3-4.

GPP IAV for 12 PFTs represented by eight products varied from 0.03 for EBF by VER to 0.38 for OSH by TG (Fig. 6c). Mean GPP IAV of multiple products showed large in OSH (0.24) and GRA (0.22) but small in EBF (0.05). Comparing Fig. 9c with 9a, it seems that those high mean annual GPP corresponds to low GPP IAV and vice versa. It is also worth noting that remarkable differences among products existed for each PFT, particularly for those PFTs with high mean GPP IAV from multiple products, such as OSH and GRA (Fig. 6c).

Among five major climate zones (A-E) defined by Köppen-Geiger, mean annual GPP of multiple products show largest values of 2461 gC m^{-2} year^{-1} in the equatorial zone (A) and the smallest values of 149 gC m^{-2} year^{-1} in the polar zone (E) (Fig. 7a). The second large mean annual GPP is mainly located in warm temperate zone (C) with 1156 gC m^{-2} year^{-1}, and the followed by boreal, D and arid, B climate zones (have roughly equivalent mean annual GPP values with 518 gC m^{-2} year^{-1} and 578 gC m^{-2} year^{-1}, respectively. Although differences among products and subzones existed, the differences in mean annual GPP between five major climate zones are more significant and dominate.

Fig. 7b showed the GPP trends for eight products in Köppen-Geiger climate zones and subzones. It is found that both climate zones C and D have relatively large trends in mean annual GPP of 3.61 and 3.04 gC m^{-2} year^{-1}, respectively. The remaining three climate zones have

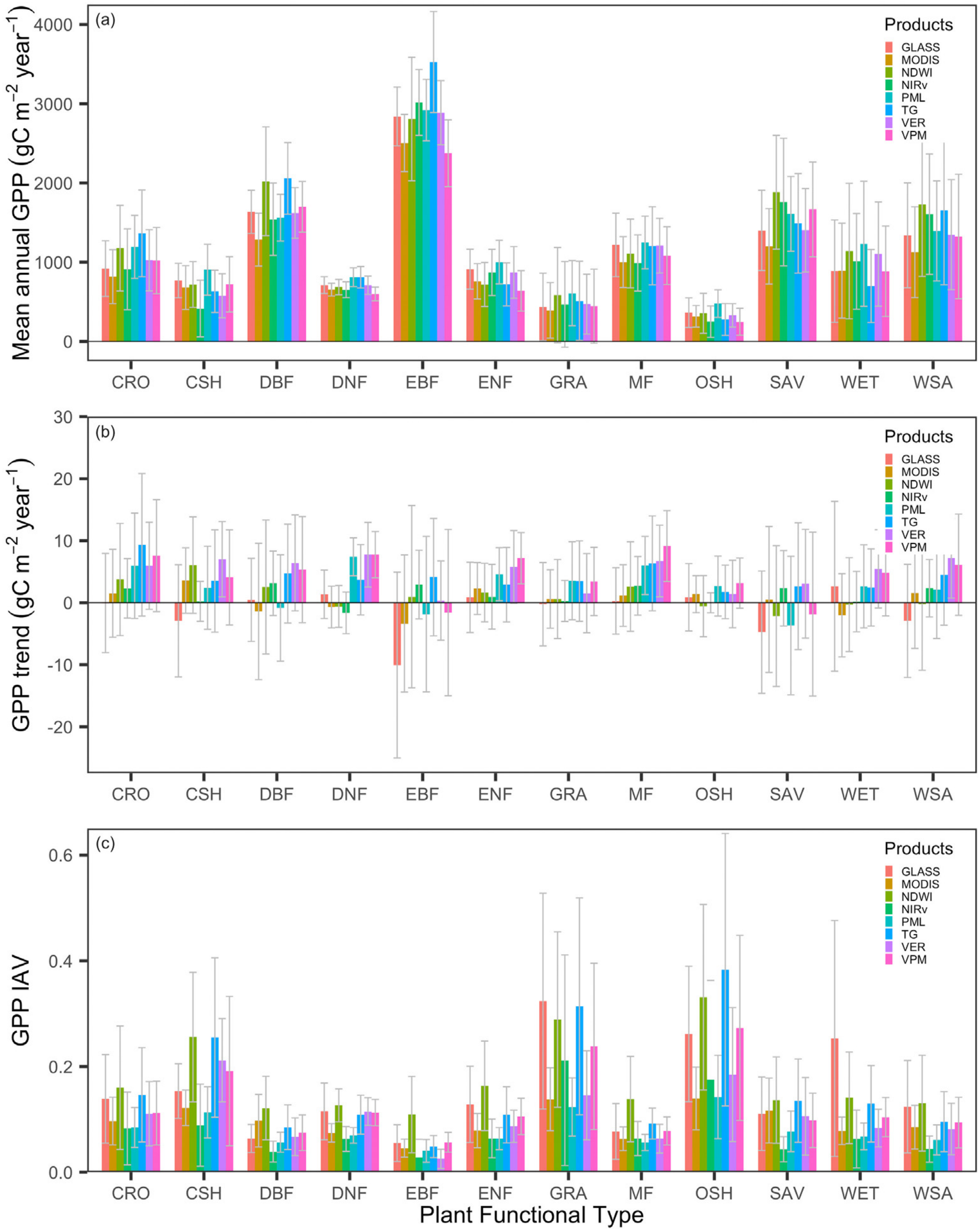

Fig. 6. Annual mean, trend and interannual variability (IAV) of GPP in 12 PFTs from eight products. The error bars represent the standard deviations.

quite smaller GPP trends of -0.82, 0.46 and 0.8 $gC\,m^{-2}\,year^{-1}$ for A, B and E, respectively. Large difference among eight GPP products existed for each climate zone. Particularly, the GPP trends simulated from GLASS and MODIS are quite different from the other five products for climate zones C and D, while for climate zones A, B and E, differences in the calculated GPP trends among products and subzones are significant.

When GPP IAV were plotted against Köppen-Geiger climate zones, it is obvious that GPP IAV in different climate subzones varied from the smallest 0.03 in subzone Af from VER product to the largest 0. 6 in subzone BWh from NDWI product. Climate zones B and E with low mean annual GPP (Fig. 7a) have relatively large mean GPP IAV of 0.28 and 0.29, respectively. While climate zones C and D have moderate mean GPP IAV of 0.12 and 0.15, respectively, and the equatorial zone (A) has the smallest mean IAV of 0.07. Similar to the variations of GPP IAV with respect to PFTs, GPP IAV for different climate subzones and among products show large difference except for the equatorial zone (A).

4. Discussion

The nature of terrestrial ecosystem primary production is the conversion of solar energy into chemical energy involving a complicated ecophysiological process driving by multiple factors from atmosphere, soil and vegetation (Beer et al., 2010). At different temporal and spatial scales, responses of GPP to these environmental variables also exhibited strong divergencies (Shi et al., 2014). Temporal divergencies are subject to the variations and trends of influencing variables, and spatial ones are subject to distribution of vegetation types, distributions and associated indicators relating to GPP (Lin et al., 2021). Both temporal and spatial issues can be reflected in the structure of a model. For example, the TG model used satellite images derived LST and EVI as driving factors (Sims et al., 2008). Although LST could represent some climatic variations, such as those in air temperature, solar radiation, vapor pressure deficit (Dong et al., 2017; Sims et al., 2008), most of their relationships with LST are non-linear and scaling them into a factorial LUE-based GPP model may lost the original correspondences of LST with other climatic variables. From this aspect, of

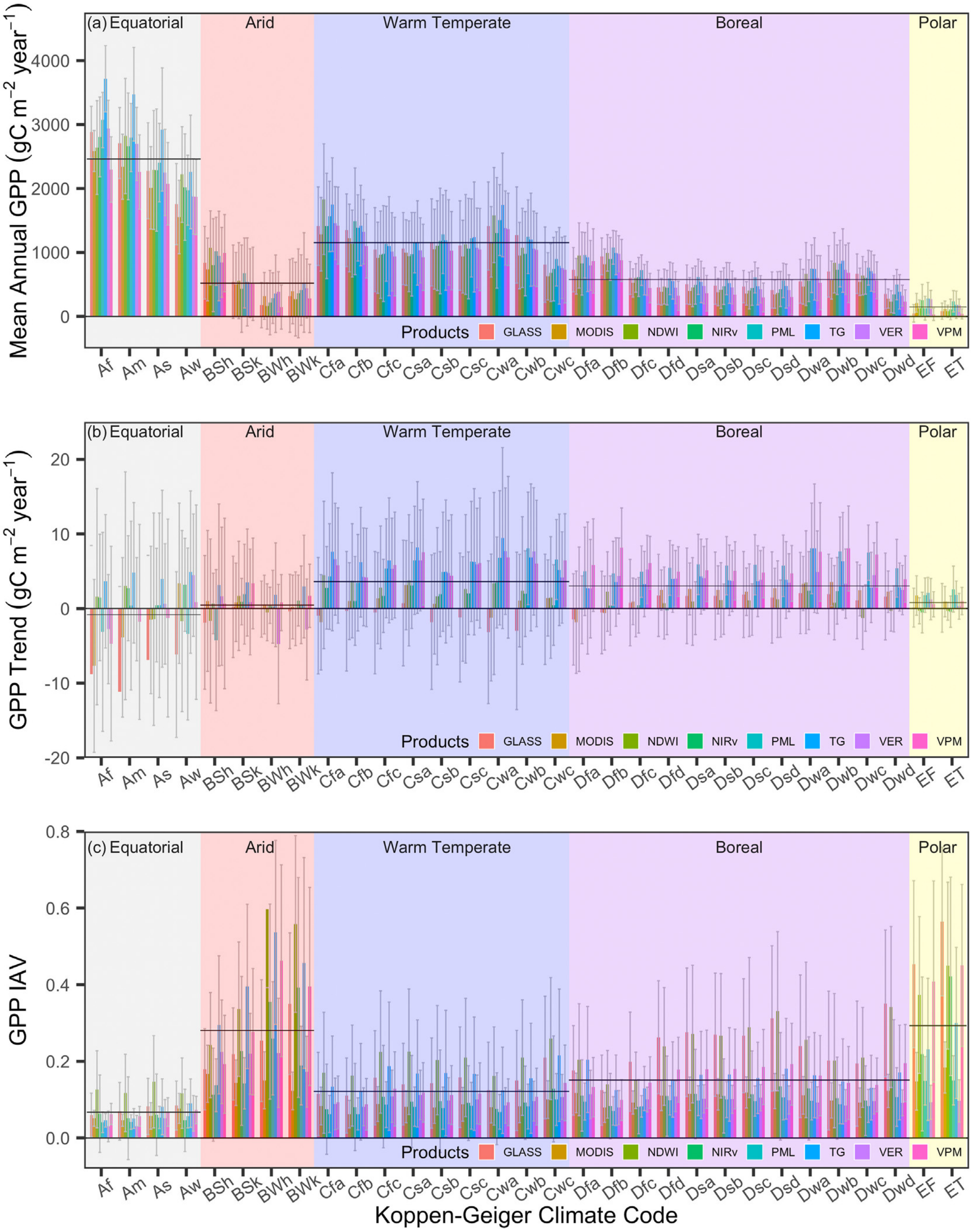

Fig. 7. Annual mean, trend and interannual variability (IAV) of GPP based on the Köppen-Geiger climate zoning map from eight products. The error bars represent the standard deviations.

the modeled GPP is largely simplified by linearly multiplying different variables that could be nolinearly related to actual GPP. Essentially, the model structure could be the most important source of uncertainties in GPP estimation (Lin et al., 2021; Zheng et al., 2020; Zheng et al., 2018). Such oversimplification also exists in other GPP models, excepted that GLASS and PML integrated more variables as inputs. The maximum LUE (ε_{max}) is a fundamental variable to construct a LUE-type GPP model. Because the eight GPP models compared in this research differ largely in their mathematic expressions (see Table 1), it is not easy to identify environmental stress on ε_{max}, which should be addressed in future efforts.

One of the advantages for remote sensing based GPP models is that a relatively consistent specific indicator can be retrieved at the global scale, and the problem of temporal divergency can be largely overcame given that sensor drifting is well corrected. The bias from remote sensing interpretation, such as the global vegetation map, can also add to the uncertainties in GPP modeling. This is particularly true for the TG model. When replacing PFT from different years, simulated mean annual GPP have significant spatial differences but does not cause significant changes in global total annual GPP. For those models which require ancillary meteorological variables, such as air temperature and vapor pressure deficit for GLASS and MODIS GPP models (Running et al., 2004). These ancillary variables may cause uncertainties in estimating GPP as well (Zhao et al., 2012; Zheng et al., 2018).

Presently, most current GPP models validated against GPP measurements from the global FLUXNET, and therefore it is relatively easy to have the estimated mean GPP values comparable. By means of some mathematic approaches such as parameter optimization (Dong et al., 2017) or machine learning (Zeng et al., 2020), consolidating the model estimate and measurement well consistent in mean GPP became more feasible. A vast number of research has reported that rising atmospheric CO_2 concentration served as fertilizer and stimulate the increase in terrestrial ecosystem GPP (Cernusak et al., 2019) but such fertilization effect of CO_2 are species-, level- and climate-dependent (Wang et al., 2020; Xie et al., 2020; Zhu et al., 2016). Further, CO_2-induced climate change can stress terrestrial GPP via the changes in temperature and precipitation (Cernusak et al., 2019). Such contrasting effects of rising atmospheric CO_2 concentration make it difficult to accurately estimate the trend of terrestrial GPP. However, the IAV of terrestrial GPP remains unclear (Piao et al., 2020) and controversial. Poulter et al. (2014) proposed that semi-arid ecosystems dominated the IAV of terrestrial carbon cycle, and Ahlström et al. (2015) further argued that semi-arid ecosystems dominated the trend of land carbon sink as well. However, based on a more comprehensive analysis, Piao et al. (2020)) insisted that it is tropical land ecosystems, rather than semi-arid ecosystems, play dominant role in regulating the IAV of global land carbon cycle. As for the driving variables of IAV of GPP, each individual variables of temperature or moisture variability or there interactions seem not to be a worldwide dominant factor (Piao et al., 2020). In a specific region, for example in Amazons, a modeling study demonstrated solar radiation was the dominant factor in regulating the IAV of tropical ecosystem GPP and temperature and precipitation also contributed but at a less extent (Ichii et al., 2005). In China, temperate monsoon precipitation was considered as the largest contributor to the IAV of land carbon cycle (Zhang et al., 2019a). However, two recent studies proposed that atmospheric vapor pressure deficit dominated the trend of terrestrial GPP (Yuan et al., 2019) and IAV of terrestrial carbon sink (He et al., 2022).

Capturing the mean, trend and IAV features of terrestrial GPP concurrently are essential standards in evaluating a model's performance. This study compared eight models in terms of the mean, trend and IAV simultaneously and found that agreement of the trend and IAV across models required large potential to make. One of possible and practical strategies is to integrate the latest advances on the mechanisms and associated environmental factors into models and to design the model's structure in terms of the diversity of biome types and climate classifications.

5. Conclusions

In this study, we made a comprehensive inter-comparison of the mean, trend and IAV of terrestrial Gross Primary Production (GPP) using eight LUE-type models which are mainly driven by remote sensing data. We found that the eight models estimated highly similar spatial patterns of mean GPP ($R > 0.9$) during the past two decades, although global total GPP still has a relatively wide range from 125 to 165 Pg year^{-1}. For the trend of GPP across the global, eight models exhibited low agreements (R ranging from 0.12 to 0.52), and seven models produced increased trends and one indicated a decreased trend. Overall, the consistencies of IAV estimated by models are larger than the trend but smaller than the mean of GPP (R ranging from 0.26 to 0.85). Both mean and IAV of GPP showed significant difference among plant functional types and climate zones. No obvious differences in GPP trends can be identified from the perspective of plant functional types. Increased trends of GPP are mainly located in warm temperate and boreal climate zones, and inter-model discrepancies are markable. We conclude that abilities of most widely used light-use-efficiency based models in estimating global terrestrial ecosystem GPP are highly consistent for the mean values, moderate consistent for IAV but quite divergent in estimating the trend. However, the GPP trend may be the mostly important concern for climate-vegetation-interaction research, particularly in the context of carbon neutrality commitment worldwide.

CRediT authorship contribution statement

Jiaqi Dong: Formal analysis, Writing – original draft, Visualization, Validation. **Longhui Li:** Conceptualization, Writing – original draft, Visualization, Validation. **Qiang Yu:** Writing – original draft, Visualization, Validation.

Declaration of competing interest

All the coauthors have agreed with the contents of this manuscript to be submitted to STOTEN. No part of the research has been published or submitted in any form elsewhere while this manuscript is being considered for publication in STOTEN. The authors declare no competing interests.

Acknowledgements

This research is supported by National Key R&D Program of China" (2017YFA0603603) and "National Natural Science Foundation of China" (42101305 and U2003201). J.Q.D also thanks the support of open fund from the Key Lab of Virtual Geographic Environment (Nanjing Normal University), Ministry of Education.

Appendix A. Supplementary data

Supplementary data to this article can be found online at https://doi.org/10.1016/j.scitotenv.2022.153343.

References

Ahlström, A., Raupach, M.R., Schurgers, G., Smith, B., Arneth, A., Jung, M., et al., 2015. The dominant role of semi-arid ecosystems in the trend and variability of the land CO2 sink. Science 348, 895.
Anav, A., Friedlingstein, P., Beer, C., Ciais, P., Harper, A., Jones, C., et al., 2015. Spatiotemporal patterns of terrestrial gross primary production: a review. Rev. Geophys. 53, 785–818.
Badgley, G., Field, C.B., Berry, J.A., 2017. Canopy near-infrared reflectance and terrestrial photosynthesis. Sci. Adv. 3, e1602244.
Badgley, G., Anderegg, L.D.L., Berry, J.A., Field, C.B., 2019. Terrestrial gross primary production: using NIRv to scale from site to globe. Glob. Chang. Biol. 25, 3731–3740.
Beer, C., Reichstein, M., Tomelleri, E., Ciais, P., Jung, M., Carvalhais, N., et al., 2010. Terrestrial gross carbon dioxide uptake: global distribution and covariation with climate. Science 329, 834.
Bonan, G.B., Lawrence, P.J., Oleson, K.W., Levis, S., Jung, M., Reichstein, M., et al., 2011. Improving canopy processes in the community land model version 4 (CLM4) using global flux fields empirically inferred from FLUXNET data. J. Geophys. Res. 116, G02014.
Canadell, J.G., Le Quere, C., Raupach, M.R., Field, C.B., Buitenhuis, E.T., Ciais, P., et al., 2007. Contributions to accelerating atmospheric CO2 growth from economic activity, carbon intensity, and efficiency of natural sinks. Proc. Natl. Acad. Sci. U. S. A. 104, 18866–18870.
Cernusak, L.A., Haverd, V., Brendel, O., Le Thiec, D., Guehl, J.-M., Cuntz, M., 2019. Robust response of terrestrial plants to rising CO2. Trends Plant Sci. 24, 578–586.
Chen, C., Park, T., Wang, X., Piao, S., Xu, B., Chaturvedi, R.K., et al., 2019a. China and India lead in greening of the world through land-use management. Nat. Sustain. 2, 122–129.
Chen, J.M., Ju, W., Ciais, P., Viovy, N., Liu, R., Liu, Y., et al., 2019b. Vegetation structural change since 1981 significantly enhanced the terrestrial carbon sink. Nat. Commun. 10, 4259.
Cox, P., Jones, C., 2008. Illuminating the modern dance of climate and CO2. Science 321, 1642.
Dai, Y., Zeng, X., Dickinson, R.E., Baker, I., Bonan, G.B., Bosilovich, M.G., et al., 2003. The common land model. Bull. Am. Meteorol. Soc. 84, 1013–1024.
Dong, J., Li, L., Shi, H., Chen, X., Luo, G., Yu, Q., 2017. Robustness and uncertainties of the "temperature and greenness" model for estimating terrestrial gross primary production. Sci. Rep. 7, 44046.
He, B., Chen, C., Lin, S., Yuan, W., Chen, H.W., Chen, D., et al., 2022. Worldwide impacts of atmospheric vapor pressure deficit on the interannual variability of terrestrial carbon sinks. Nat. Sci. Rev., nwab150 https://doi.org/10.1093/nsr/nwab150 In press.
Ichii, K., Hashimoto, H., Nemani, R., White, M., 2005. Modeling the interannual variability and trends in gross and net primary productivity of tropical forests from 1982 to 1999. Glob. Planet. Chang. 48, 274–286.
Krinner, G., Viovy, N., de Noblet-Ducoudré, N., Ogée, J., Polcher, J., Friedlingstein, P., et al., 2005. A dynamic global vegetation model for studies of the coupled atmosphere-biosphere system. Glob. Biogeochem. Cycl. 19.
Landsberg, J.J., Waring, R.H., 1997. A generalised model of forest productivity using simplified concepts of radiation-use efficiency, carbon balance and partitioning. For. Ecol. Manag. 95, 209–228.
Law, R.M., Ziehn, T., Matear, R.J., Lenton, A., Chamberlain, M.A., Stevens, L.E., et al., 2015. The carbon cycle in the australian community climate and earth system simulator (ACCESS-ESM1) – part 1: model description and pre-industrial simulation. Geosci. Model Dev. Discuss. 8, 8063–8116.
Li, Y., Li, L., Dong, J., Bai, J., Yuan, X., Song, S., et al., 2020. Process refinement contributed more than parameter optimization to improve the CoLM's performance in simulating the carbon and water fluxes in a grassland. Agric. For. Meteorol. 291, 108067.
Lin, S., Li, J., Liu, Q., Gioli, B., Paul-Limoges, E., Buchmann, N., et al., 2021. Improved global estimations of gross primary productivity of natural vegetation types by incorporating plant functional type. Int. J. Appl. Earth Obs. Geoinf. 100, 102328.
Myneni, R.B., Williams, D.L., 1994. On the relationship between FAPAR and NDVI. Remote Sens. Environ. 49, 200–211.

Peel, M.C., Finlayson, B.L., McMahon, T.A., 2007. Updated world map of the Köppen-Geiger climate classification. Hydrol. Earth Syst. Sci. 11, 1633–1644.
Piao, S., Wang, X., Wang, K., Li, X., Bastos, A., Canadell, J.G., et al., 2020. Interannual variation of terrestrial carbon cycle: issues and perspectives. Glob. Chang. Biol. 26, 300–318.
Potter, C.S., Randerson, J.T., Field, C.B., Matson, P.A., Vitousek, P.M., Mooney, H.A., et al., 1993. Terrestrial ecosystem production: a process model based on global satellite and surface data. Glob. Biogeochem. Cycl. 7, 811–841.
Poulter, B., Frank, D., Ciais, P., Myneni, R.B., Andela, N., Bi, J., et al., 2014. Contribution of semi-arid ecosystems to interannual variability of the global carbon cycle. Nature 509, 600–603.
Rascher, U., Alonso, L., Burkart, A., Cilia, C., Cogliati, S., Colombo, R., et al., 2015. Sun-induced fluorescence – a new probe of photosynthesis: first maps from the imaging spectrometer HyPlant. Glob. Chang. Biol. 21, 4673–4684.
Running, S., Nemani, R., Heinsch, F., Zhao, M., Reever, M., Hashimoto, H., 2004. A continuous satellite-derived measure of global terrestrial primary production. Bioscience 54 (547–560), 14.
Schaefer, K., Collatz, G.J., Tans, P., Denning, A.S., Baker, I., Berry, J., et al., 2008. Combined simple Biosphere/Carnegie-Ames-Stanford approach terrestrial carbon cycle model. J. Geophys. Res.Biogeosci. 113.
Shi, H., Li, L., Eamus, D., Cleverly, J., Huete, A., Beringer, J., et al., 2014. Intrinsic climate dependency of ecosystem light and water-use-efficiencies across Australian biomes. Environ. Res. Lett. 9, 104002.
Sims, D.A., Rahman, A.F., Cordova, V.D., El-Masri, B.Z., Baldocchi, D.D., Flanagan, L.B., et al., 2006. On the use of MODIS EVI to assess gross primary productivity of North American ecosystems. J. Geophys. Res. Biogeosci. 111, G04015.
Sims, D.A., Rahman, A.F., Cordova, V.D., El-Masri, B.Z., Baldocchi, D.D., Bolstad, P.V., et al., 2008. A new model of gross primary productivity for North American ecosystems based solely on the enhanced vegetation index and land surface temperature from MODIS. Remote Sens. Environ. 112, 1633–1646.
Sitch, S., Friedlingstein, P., Gruber, N., Jones, S.D., Murray-Tortarolo, G., Ahlström, A., et al., 2013. Trends and drivers of regional sources and sinks of carbon dioxide over the past two decades. Biogeosci. Discuss. 10, 20113–20177.
Sitch, S., Friedlingstein, P., Gruber, N., Jones, S.D., Murray-Tortarolo, G., Ahlström, A., et al., 2015. Recent trends and drivers of regional sources and sinks of carbon dioxide. Biogeosciences 12, 653–679.
Wang, S., Zhang, Y., Ju, W., Chen, J.M., Ciais, P., Cescatti, A., et al., 2020. Recent global decline of CO2 fertilization effects on vegetation photosynthesis. Science 370, 1295–1300.
Wang, S., Zhang, Y., Ju, W., Qiu, B., Zhang, Z., 2021a. Tracking the seasonal and inter-annual variations of global gross primary production during last four decades using satellite near-infrared reflectance data. Sci. Total Environ. 755, 142569.
Wang, Y.P., Law, R.M., Pak, B., 2010. A global model of carbon, nitrogen and phosphorus cycles for the terrestrial biosphere. Biogeosciences 7, 2261–2282.
Wang, Y.P., Lu, X.J., Wright, I.J., Dai, Y.J., Rayner, P.J., Reich, P.B., 2012. Correlations among leaf traits provide a significant constraint on the estimate of global gross primary production. Geophys. Res. Lett. 39 n/a-n/a.
Wang, Z., Liu, S., Wang, Y.-P., Valbuena, R., Wu, Y., Kutia, M., et al., 2021;. Tighten the bolts and nuts on GPP estimations from sites to the globe: an assessment of remote sensing based LUE models and supporting data fields. Remote Sens. 13.
Williams, M., Richardson, A.D., Reichstein, M., Stoy, P.C., Peylin, P., Verbeeck, H., et al., 2009. Improving land surface models with FLUXNET data. Biogeosciences 6, 1341–1359.
Xiao, X., Zhang, Q., Braswell, B., Urbanski, S., Boles, S., Wofsy, S., et al., 2004. Modeling gross primary production of temperate deciduous broadleaf forest using satellite images and climate data. Remote Sens. Environ. 91, 256–270.
Xie, S., Mo, X., Hu, S., Liu, S., 2020. Contributions of climate change, elevated atmospheric CO2 and human activities to ET and GPP trends in the three-north region of China. Agric. For. Meteorol. 295, 108183.
Yuan, W., Liu, S., Zhou, G., Zhou, G., Tieszen, L.L., Baldocchi, D., et al., 2007. Deriving a light use efficiency model from eddy covariance flux data for predicting daily gross primary production across biomes. Agric. For. Meteorol. 143, 189–207.
Yuan, W., Cai, W., Xia, J., Chen, J., Liu, S., Dong, W., et al., 2014. Global comparison of light use efficiency models for simulating terrestrial vegetation gross primary production based on the LaThuile database. Agric. For. Meteorol. 192–193, 108–120.
Yuan, W., Zheng, Y., Piao, S., Ciais, P., Lombardozzi, D., Wang, Y., et al., 2019. Increased atmospheric vapor pressure deficit reduces global vegetation growth. ScienceAdvances 5, eaax1396.
Zeng, J., Matsunaga, T., Tan, Z.-H., Saigusa, N., Shirai, T., Tang, Y., et al., 2020. Global terrestrial carbon fluxes of 1999–2019 estimated by upscaling eddy covariance data with a random forest. Sci. Data 7, 313.
Zeng, X., Shaikh, M., Dai, Y., Dickinson, R.E., Myneni, R., 2002. Coupling of the common land model to the NCAR Community climate model. J. Clim. 15, 1832–1854.
Zhang, L., Ren, X., Wang, J., He, H., Wang, S., Wang, M., et al., 2019a. Interannual variability of terrestrial net ecosystem productivity over China: regional contributions and climate attribution. Environ. Res. Lett. 14, 014003.
Zhang, Y., Peña-Arancibia, J.L., McVicar, T.R., Chiew, F.H.S., Vaze, J., Liu, C., et al., 2016. Multi-decadal trends in global terrestrial evapotranspiration and its components. Sci. Rep. 6, 19124.
Zhang, Y., Xiao, X., Wu, X., Zhou, S., Zhang, G., Qin, Y., et al., 2017. A global moderate resolution dataset of gross primary production of vegetation for 2000–2016. Sci. Data 4, 170165.
Zhang, Y., Kong, D., Gan, R., Chiew, F.H.S., McVicar, T.R., Zhang, Q., et al., 2019b. Coupled estimation of 500 m and 8-day resolution global evapotranspiration and gross primary production in 2002–2017. Remote Sens. Environ. 222, 165–182.
Zhao, Y., Ciais, P., Peylin, P., Viovy, N., Longdoz, B., Bonnefond, J.M., et al., 2012. How errors on meteorological variables impact simulated ecosystem fluxes: a case study for six french sites. Biogeosciences 9, 2537–2564.
Zheng, Y., Zhang, L., Xiao, J., Yuan, W., Yan, M., Li, T., et al., 2018. Sources of uncertainty in gross primary productivity simulated by light use efficiency models: model structure, parameters, input data, and spatial resolution. Agric. For. Meteorol. 263, 242–257.
Zheng, Y., Shen, R., Wang, Y., Li, X., Liu, S., Liang, S., et al., 2020. Improved estimate of global gross primary production for reproducing its long-term variation, 1982–2017. Earth Syst. Sci. Data 12, 2725–2746.
Zhu, Z., Piao, S., Myneni, R.B., Huang, M., Zeng, Z., Canadell, J.G., et al., 2016. Greening of the earth and its drivers. Nat. Clim. Chang. 6, 791–795.